Journal of Computational and Applied Mathematics 336 (2018) 235–248

Contents lists available at ScienceDirect

Journal of Computational and Applied Mathematics

journal homepage: www.elsevier.com/locate/cam

A combined finite element method for elliptic problems posted in domains with rough boundaries

Shipeng Xu, Weibing Deng *, Haijun Wu *

Department of Mathematics, Nanjing University, Nanjing 210093, People's Republic of China

ARTICLE INFO

Article history:
Received 16 February 2017
Received in revised form 28 October 2017

MSC:
34E13
65N15
65N30

Keywords:
Combined finite element method
Rough boundary
Penalty technique

ABSTRACT

A combined finite element method is presented in this paper to solve the elliptic problems posted in domains with rough boundaries. Solving these problems numerically is difficult because resolving the boundaries usually requires very fine meshes, while good quality meshes often over-refine unnecessarily the interior of the domain. The basic idea of the proposed method is to use a fine mesh with size h in the vicinity of oscillating boundaries and a coarse mesh with size $H \gg h$ for other portions of the domain to reduce some unnecessary computational effort. The transmission conditions across the fine-coarse mesh interface are treated by the penalty technique. The key point of the method lies in the new scheme employing a weighted average in the definition of the bilinear form, which avoids the affection of the ratio H/h in the error estimate. We prove a quasi-optimal convergence in terms of elements since there is no whole H^2 regularity in the domain with rough boundaries. Numerical results are provided for elliptic equations in domains with non-oscillating or oscillating boundaries to illustrate the theoretical results.

1. Introduction

Many problems arising in modern material sciences and engineering are described by partial differential equations in domains with very rough boundaries. Typical examples include the electromagnetic scattering by an obstacle coated with an absorbing inhomogeneous paint, the dynamics of two-fluid flow in porous media and past rough walls, the hydrodynamic lubrication of rough surfaces, and among many others (see [1–3] and the references therein). Solving these problems numerically can be hard because resolving the boundaries usually requires very fine meshes and hence tremendous amount of computer memory and CPU time. To overcome this difficulty, many papers have been devoted to the homogenization of boundary value problems in domains with fast oscillating boundaries (see [4–6,1] and the references therein). In general, the homogenized problems are the boundary value problems for the same equations in the same domains but with the mollified boundary instead of the oscillating one. The mollified boundary and the effective boundary condition on it are determined by the original boundary condition and the geometry of the oscillations.

The homogenization theory mainly studied the identification of the homogenized problems and proving the convergence theorems for the solutions. To our knowledge, less work of multiscale methods has been done for the boundary value problems in a domain with multiscale boundary. Only recently, some researchers began to concern about this topic. See, for example, the multiscale finite element method (MsFEM) for Laplace equation with homogeneous Dirichlet boundary value on rough domain [7], the MsFEM for Laplace equation with oscillating Neumann boundary conditions on rough boundaries [8], and the multiscale methods based on the localized orthogonal decomposition (LOD) technique for problems

* Corresponding authors.
E-mail addresses: xushipeng@smail.nju.edu.cn (S. Xu), wbdeng@nju.edu.cn (W. Deng), hjw@nju.edu.cn (H. Wu).

https://doi.org/10.1016/j.cam.2017.12.049
0377-0427/

with complex geometry [9]. Just as the classical MsFEM [10], the author in [7] defines the multiscale basis functions for the elements near the rough boundary by solving a cell problem with the homogeneous Dirichlet condition on the rough edge and with linear nodal basis function as boundary condition on other edges. By this way, the influence of the geometry should be captured by the basis functions. The MsFEM in [8] introduces a special Neumann boundary condition that incorporates both the microscopically geometrical and physical information of the rough boundary for the local cell problem posed on elements with rough edge. Compared to the method in [7], this approach can be applied to problems with non-Dirichlet boundary conditions or problems with inhomogeneous Dirichlet boundary value over the rough boundary. However, the analysis in [7,8] is limited to periodic data. In [9], the multiscale analysis based on the LOD technique is extended to elliptic problems on domains with cracks or complicated boundary, in which corrected coarse test and trail spaces taking the fine features of the domain into account are constructed. We remark that all of the above mentioned methods are based on solutions of local problems which can be computed off-line and can thus be done in parallel. However, these methods are still expensive since local problems depend on the small parameter that characterizes the roughness of the boundary. Of course, all these methods are much cheaper than using pure piecewise linear FEM in the whole domain.

The oscillation of the boundary also stands for a kind of scale, which are subject to multiscale problems (see [11,9,8]). For such problem, since the global regularity of the solution is low (especially near the boundary), the traditional finite element method (FEM) becomes inapplicable because resolving the boundaries usually requires very fine meshes, and good quality meshes often over-refine unnecessarily the interior of the domain. Thus, in this paper, we try to introduce a combined finite element method (combined FEM) which uses a fine mesh with size h in the vicinity of oscillating boundary while uses a coarse mesh with size $H(\gg h)$ for the interior subdomains. By this way, we can cut down some unnecessary computational effort. The negative effect of the processing method is that the generated mesh has many hanging nodes along the fine-coarse mesh interface. For instance, here for each edge of the interface coarse-element, it has $(H/h - 2)$ hanging nodes. Along the interface, the numerical solution is discontinuous. Thanks to the penalty techniques used in the interior penalty discontinuous (or continuous) Galerkin methods originated in 1970s [12–17], we may deal with the transmission condition across the fine-coarse mesh interface by penalizing the jumps from the function values of the finite element solution on the fine mesh to those on the coarse mesh. However, if we use the traditional variational form with the arithmetic average of the function values from the fine and coarse grids respectively, the error analysis shows that the ratio H/h debases the convergence rate (see [16,18]). Hence, in the proposed scheme, we employ a weighted average in the definition of the bilinear form, which can eliminate the affection of the ratio H/h in the error estimates. The weighted coefficients are depended on the sizes of coarse and fine meshes along the interface, namely H and h. The penalty coefficient is defined as $\gamma/(H + h)$ for some positive constant γ. We prove a quasi-optimal convergence in terms of elements since for the rough boundary problem its solution is generally in $H^s(\Omega)$ with $1 < s < 2$.

There are some other numerical methods to handle the complex geometrical boundary such as the cut finite element method in [19] where the boundary and interface conditions are built into the discrete formulation by the Nitsche's method, the extended/generalized finite element method in [20] which is achieved by adding special shape functions to the polynomial approximation space of the classical finite element method, and the composite finite elements in [21]. The composite finite element method which constructs a coarse basis that is fitted to the boundary has been successfully applied to problems in domain with oscillating boundaries (see [22–24]).

Besides problems with oscillating boundaries, our method may be applied into other partial differential equations with challenging singularities, e.g., well problems with the Dirac function singularities, partial differential equations on domains containing small geometric details, high conductivity channels which appear in many fields of science and engineering. It is also possible to combine the present method with the standard MsFEM to deal with the problems with both oscillating coefficients and oscillating boundary data. Note that a lot of ways have been developed to deal with the multiscale problems with singularities, such as, the MsFEMs (see [25–31]) and the localized orthogonal decomposition methods (see [32–35]). The proposed method is very similar to the combined MsFEM introduced in [30], which uses the traditional linear FEM directly on a fine mesh of the problematic part of the domain and the oversampling MsFEM on a coarse mesh of the other part to solve the multiscale problems with singularities.

The outline of the paper is as follows. In Section 2, we describe the model problem and introduce the combined FEM. In Section 3, we analyze the proposed method, including the continuity, the coercivity of the scheme, and the bound of the error in energy norm which shows that there is no ratio H/h appearing in the error estimate and the convergence order is quasi-optimal with respect to elements. In Section 4, we simulate some model problems in the domain with rough boundaries by the combined FEM. The numerical experiments verify the theoretical results. We end with some conclusions which are drawn in Section 5.

Throughout the paper, C, γ' and γ are used to denote the generic positive constants which are independent of H, h and maybe depend on some constant parameters (e.g., penalty parameter γ), which are different in different places. We also use the shorthand notation $A \lesssim B$ and $B \gtrsim A$ for the inequality $A \leq CB$ and $B \geq CA$ respectively. The notation $A \eqsim B$ is equivalent to the statement $A \lesssim B$ and $B \lesssim A$.

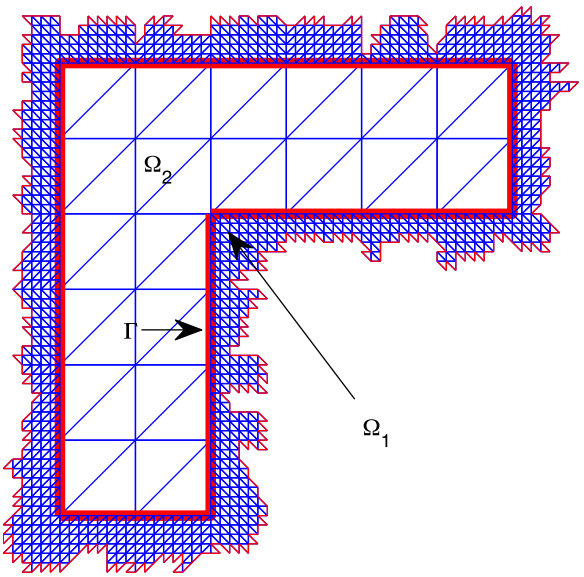

Fig. 1. A diagram of the space discretization.

2. The combined finite element method

2.1. Model problem

Consider the following second order elliptic equation:

$$\begin{aligned} -\nabla \cdot (A\nabla u) &= f \qquad \text{in } \Omega, \\ u &= 0 \qquad \text{on } \partial\Omega, \end{aligned} \tag{2.1}$$

where $\Omega \subset \mathbb{R}^d$ $(d = 2, 3)$ is a bounded convex or nonconvex domain with Lipschitz boundary. Assume the source term $f \in L^2(\Omega)$, and the matrix $A(x) = [a_{ij}(x)] \in (W^{1,\infty}(\Omega))^{d\times d}$ is symmetric and satisfies the uniformly elliptic condition that there exist two constants λ, $\Lambda > 0$ such that

$$\lambda|\xi|^2 \le a_{ij}(x)\xi_i\xi_j \le \Lambda|\xi|^2 \quad \forall \xi \in \mathbb{R}^d. \tag{2.2}$$

Note that the boundary $\partial\Omega$ of the domain Ω may be oscillating, which may possess the complex geometrical structure. In this paper, we try to design the numerical method for complicate geometry which is quite general in the sense that we do not impose any assumptions on the oscillating of the boundary. Hence, we have not given any detailed characterization of the so-called complicate geometry. However, for further theoretical analysis, we give some regularity assumption which can be seen as the starting point of the method. We assume that the regularity of the solution in the interior of the domain Ω is H^2, while the local regularity of the solution in vicinity of the boundary $\partial\Omega$ is H^{1+s} with $0 < s \le 1$. The concrete illustration of the regularity of the solution will be given later. As mentioned above, for problems in rough domain, the traditional FEM needs meshes fine enough to resolve the multiscale boundary, and good quality meshes often over-refine unnecessarily the interior of the domain. Note that, for simplicity, we consider only the homogeneous Dirichlet boundary condition while the extension to non-homogeneous one is obvious and is omitted.

2.2. Space discretization

In order to reduce some unnecessary computational effort spending on the interior domain, we first separate the research area Ω into two subdomains Ω_1 and Ω_2 such that $\Omega_2 \subset\subset \Omega$ and $\Omega = \Omega_1 \cup \Omega_2 \cup \Gamma$, where $\Gamma = \partial\Omega_1 \cap \partial\Omega_2$ is the interface of Ω_1 and Ω_2 (see Fig. 1 for an illustration). Throughout the paper, we shall use the standard Sobolev space $H^s(\Omega)$, its norm and inner product, and refer to [36,37] for their definitions.

For simplicity, we assume that the length/area of Γ satisfies $|\Gamma| = O(1)$, and Γ is Lipschitz continuous. Let $\mathcal{T}_h$ and $\mathcal{T}_H$ be the shape-regular and quasi-uniform triangulations of the domain Ω_1 and Ω_2 respectively, which constitute a triangulation $\mathcal{T}_{h,H}$ of Ω. Denote Γ_h and Γ_H the two partitions of the interface Γ introduced by $\mathcal{T}_h$ and $\mathcal{T}_H$, respectively. For any element $K \in \mathcal{T}_{h,H}$, we define h_K (or H_K) as diam(K). Denote $h = \max_{K\in\mathcal{T}_h} h_K$, $H = \max_{K\in\mathcal{T}_H} H_K$. $\mathbf{n}$ denotes outward normal vector on

Γ pointing from Ω_1 to Ω_2, while $\mathbf{n}_i$ denotes outside normal vector of Ω_i, $i = 1, 2$. Let $\mathcal{T}_h^\Gamma$ be the set of elements in $\mathcal{T}_h$ whose intersections with Γ are theirs faces, that is,

$$\mathcal{T}_h^\Gamma := \{K : K \in \mathcal{T}_h \text{ whose one face} \subset \Gamma\}.$$

Let

$$\widetilde{\mathcal{T}}_h := \mathcal{T}_h \setminus \mathcal{T}_h^\Gamma.$$

For $s \geq 0$ and any subset $\mathcal{M} \subset \mathcal{T}_{h,H}$, denote $H^s(\mathcal{M}) := \prod_{K\in\mathcal{M}} H^s(K)$ and

$$|\cdot|^2_{s,\mathcal{M}} := \sum_{K\in\mathcal{M}} |\cdot|^2_{s,K}.$$

Next we define the average and jump on Γ. Let v be a piecewise smooth function and let $e \in \Gamma$ be a face (if $d = 2$, face means edge) shared by two neighboring elements K_1 in Ω_1 and K_2 in Ω_2. If we denote by v_i the trace of v taken from within K_i, $i = 1, 2$, then the weighted averages $\{v\}_w$, $\{v\}^w$, and the jump $[v]$ of v over e are defined by

$$\{v\}_w = w_1 v_1 + w_2 v_2, \quad \{v\}^w = w_2 v_1 + w_1 v_2, \quad [v] = v_1 - v_2, \tag{2.3}$$

where the weights

$$w_1 = \frac{h}{H+h} \text{ and } w_2 = \frac{H}{H+h}.$$

For example, here we have

$$\{(A\nabla v)\cdot\mathbf{n}\}_w = w_1(A\nabla v_1)\cdot\mathbf{n} + w_2(A\nabla v_2)\cdot\mathbf{n}. \tag{2.4}$$

To present the combined FEM formulation, we introduce the following "energy" space:

$$\begin{aligned} V = \{v \in L^2(\Omega) : v|_{\Omega_i} \in H^1(\Omega_i), i = 1, 2, v|_{\partial\Omega} = 0, \\ v|_K \in H^2(K), \forall K \in \mathcal{T}_{h,H}, K \cap \Gamma \neq \emptyset\}. \end{aligned} \tag{2.5}$$

Denote by V_H and V_h the H^1-conforming linear finite element space over $\mathcal{T}_H$ and $\mathcal{T}_h$ respectively. For a given mesh $\mathcal{T}_{h,H}$, we define the corresponding finite element space for the combined FEM as follows:

$$V_{h,H} = \{v \in L^2(\Omega) : v|_{\Omega_1} \in V_h, v|_{\Omega_2} \in V_H, v|_{\partial\Omega} = 0\}. \tag{2.6}$$

2.3. Formulations of the combined FEM

Testing Eq. (2.1) by any $v \in V$, using integration by parts, and using the "magic" formula $[ab] = \{a\}_w[b] + [a]\{b\}^w$, we obtain

$$\int_{\Omega_1\cup\Omega_2} A\nabla u\cdot\nabla v - \int_\Gamma \{(A\nabla u)\cdot\mathbf{n}\}_w[v] = \int_{\Omega_1\cup\Omega_2} fv.$$

Introduce the following bilinear form on $V \times V$:

$$\begin{aligned} a(u, v) = \int_{\Omega_1\cup\Omega_2} A\nabla u\cdot\nabla v - \int_\Gamma \{(A\nabla u)\cdot\mathbf{n}\}_w[v] - \beta\int_\Gamma [u]\{(A\nabla v)\cdot\mathbf{n}\}_w \\ + \int_\Gamma \frac{\gamma}{H+h}[u][v], \end{aligned} \tag{2.7}$$

where β is a real number such as -1, 0, 1, and $\gamma > 0$ will be specified later. Clearly,

$$a(u, v) = (f, v) := \int_\Omega fv \quad \forall v \in V. \tag{2.8}$$

Then, our combined FEM is to find $u_{h,H} \in V_{h,H}$ such that

$$a(u_{h,H}, v_{h,H}) = (f, v_{h,H}) \qquad \forall v_{h,H} \in V_{h,H}. \tag{2.9}$$

In order to estimate the error of the combined FEM solution, we introduce the following energy norm on the space V:

$$\begin{aligned} |||v||| := \Bigg(\left\|A^{1/2}\nabla v\right\|^2_{0,\Omega_1\cup\Omega_2} + \frac{\gamma}{H+h}\|[v]\|^2_{0,\Gamma} \\ + \frac{H+h}{\gamma}\|\{A\nabla v\cdot\mathbf{n}\}_w\|^2_{0,\Gamma}\Bigg)^{1/2} \qquad \forall v \in V. \end{aligned} \tag{2.10}$$

3. Error estimates

For the combined FEM, we first show the stability of the bilinear form guaranteeing the existence and uniqueness of the solution, and then prove the error estimate with $\beta = 1$. For other cases such as $\beta = -1, 0$, the analysis is similar and is omitted here.

The following three inequalities will be used frequently in this paper (cf. [37]). They are the trace inequality:

$$\|v\|_{0,\partial K} \lesssim h_K^{-\frac{1}{2}} \|v\|_{0,K} + h_K^{\frac{1}{2}} \|\nabla v\|_{0,K} \quad \forall v \in H^1(K), K \in \mathcal{T}_{h,H}, \tag{3.1}$$

the inverse trace inequality:

$$\|v\|_{0,\partial K} \leq C_{\mathrm{tr}} h_K^{-\frac{1}{2}} \|v\|_{0,K} \quad \forall v \in P_1(K), K \in \mathcal{T}_{h,H} \tag{3.2}$$

for some constant C_{tr} independent of K and v, and Young's inequality:

$$\forall \varepsilon > 0, \quad \forall a, b \in \mathbb{R}, \quad ab \leq \frac{\varepsilon}{2} a^2 + \frac{1}{2\varepsilon} b^2. \tag{3.3}$$

3.1. Céa's Lemma

The following lemma gives the continuity and coercivity of the bilinear form $a(\cdot,\cdot)$ for the combined FEM:

Lemma 3.1. *There exists a constant γ_0 independent of H, h such that when $\gamma \geq \gamma_0$, it holds that*

$$|a(u, v)| \leq 2 |||u||| \, |||v||| \quad \forall u, v \in V, \tag{3.4}$$

$$a(v_{h,H}, v_{h,H}) \geq \frac{1}{2} \left|\left|\left| v_{h,H} \right|\right|\right|^2 \quad \forall v_{h,H} \in V_{h,H}. \tag{3.5}$$

Proof. (3.4) can be proven by Cauchy–Schwarz inequality directly. Next, we prove (3.5). Denote $v_h = v_{h,H}|_{\Omega_1}$ and $v_H = v_{h,H}|_{\Omega_2}$. By use of the inverse trace inequality (3.2) and the uniformly elliptic condition (2.2), it follows that

$$\begin{aligned}
&\frac{H+h}{\gamma} \left\| \{A\nabla v_{h,H} \cdot \mathbf{n}\}_w \right\|_{0,\Gamma}^2 \leq 2 \sum_{e \in \Gamma_h} w_1 \frac{H+h}{\gamma} \|A\nabla v_h\|_{0,e}^2 \\
&\quad + 2 \sum_{E \in \Gamma_H} w_2 \frac{H+h}{\gamma} \|A\nabla v_H\|_{0,E}^2 \\
&\leq \frac{2\Lambda^2}{\gamma} \sum_{e \in \Gamma_h} h \|\nabla v_h\|_{0,e}^2 + \frac{2\Lambda^2}{\gamma} \sum_{E \in \Gamma_H} H \|\nabla v_H\|_{0,E}^2 \\
&\leq \frac{2\Lambda^2 C_{\mathrm{tr}}}{\gamma} \sum_{K \in \mathcal{T}_h} \|\nabla v_h\|_{0,K}^2 + \frac{2\Lambda^2 C_{\mathrm{tr}}}{\gamma} \sum_{K \in \mathcal{T}_H} \|\nabla v_H\|_{0,K}^2 \\
&\leq \frac{2\Lambda^2 C_{\mathrm{tr}}}{\lambda\gamma} \sum_{K \in \mathcal{T}_h} \left\| A^{1/2} \nabla v_h \right\|_{0,K}^2 + \frac{2\Lambda^2 C_{\mathrm{tr}}}{\lambda\gamma} \sum_{K \in \mathcal{T}_H} \left\| A^{1/2} \nabla v_H \right\|_{0,K}^2 \\
&= \frac{2\Lambda^2 C_{\mathrm{tr}}}{\lambda\gamma} \sum_{K \in \mathcal{T}_{h,H}} \left\| A^{1/2} \nabla v_{h,H} \right\|_{0,K}^2 .
\end{aligned} \tag{3.6}$$

Further, applying the Young's inequality (3.3), we obtain

$$\begin{aligned}
a(v_{h,H}, v_{h,H}) &= \left|\left|\left| v_{h,H} \right|\right|\right|^2 - 2 \int_\Gamma \{A\nabla v_{h,H} \cdot \mathbf{n}\}_w [v_{h,H}] \mathrm{d}s \\
&\quad - \frac{H+h}{\gamma} \left\| \{A\nabla v_{h,H} \cdot \mathbf{n}\}_w \right\|_{0,\Gamma}^2 \\
&\geq \left|\left|\left| v_{h,H} \right|\right|\right|^2 - \frac{1}{2} \frac{\gamma}{H+h} \left\| [v_{h,H}] \right\|_{0,\Gamma}^2 - 3 \frac{H+h}{\gamma} \left\| \{A\nabla v_{h,H} \cdot \mathbf{n}\}_w \right\|_{0,\Gamma}^2 \\
&\geq \left|\left|\left| v_{h,H} \right|\right|\right|^2 - \frac{1}{2} \frac{\gamma}{H+h} \left\| [v_{h,H}] \right\|_{0,\Gamma}^2 - \frac{6\Lambda^2 C_{\mathrm{tr}}}{\lambda\gamma} \left\| A^{1/2} \nabla v_{h,H} \right\|_{0,\Omega_1 \cup \Omega_2}^2 \\
&\geq \left(1 - \max\left(\frac{1}{2}, \frac{6\Lambda^2 C_{\mathrm{tr}}}{\lambda\gamma} \right) \right) \left|\left|\left| v_{h,H} \right|\right|\right|^2 .
\end{aligned}$$

Then (3.5) follows by taking sufficiently large γ_0 such that $\frac{6\Lambda^2 C_{\mathrm{tr}}}{\lambda\gamma_0} \leq \frac{1}{2}$. The proof of the lemma is completed. □

The following lemma is an analogue of the Céa lemma [37].

Lemma 3.2. *Let u and $u_{h,H}$ be the solutions of (2.1) and (2.9) respectively. There exists a constant $\gamma_0 > 0$ independent of H and h such that when $\gamma \geq \gamma_0$, it holds:*

$$\left|\!\left|\!\left| u - u_{h,H} \right|\!\right|\!\right| \lesssim \inf_{v_{h,H} \in V_{h,H}} \left|\!\left|\!\left| u - v_{h,H} \right|\!\right|\!\right|. \tag{3.7}$$

Proof. From (2.8) and (2.9), we have the following Galerkin orthogonality:

$$a(u - u_{h,H}, v_{h,H}) = 0 \qquad \forall v_{h,H} \in V_{h,H}. \tag{3.8}$$

Then from (3.5) it follows that

$$\begin{aligned} \left|\!\left|\!\left| u_{h,H} - v_{h,H} \right|\!\right|\!\right|^2 &\leq 2a(u_{h,H} - v_{h,H}, u_{h,H} - v_{h,H}) \\ &= 2a(u - v_{h,H}, u_{h,H} - v_{h,H}) \\ &\leq 4 \left|\!\left|\!\left| u - v_{h,H} \right|\!\right|\!\right| \left|\!\left|\!\left| u_{h,H} - v_{h,H} \right|\!\right|\!\right|. \end{aligned}$$

Hence, it follows from the triangle inequality that

$$\left|\!\left|\!\left| u - u_{h,H} \right|\!\right|\!\right| \leq \left|\!\left|\!\left| u - v_{h,H} \right|\!\right|\!\right| + \left|\!\left|\!\left| u_{h,H} - v_{h,H} \right|\!\right|\!\right| \leq 5 \left|\!\left|\!\left| u - v_{h,H} \right|\!\right|\!\right|.$$

This completes the proof of the lemma. □

3.2. General polyhedral boundary

Let $I_H : C(\bar{\Omega}_2) \mapsto V_H$ be the standard Lagrange interpolation operator. It is well known that (see, e.g., [36])

$$|v - I_H v|_{i,\mathcal{T}_H} \lesssim H^{2-i} |v|_{2,\mathcal{T}_H}, \quad 0 \leq i \leq 2, \ \forall v \in H^2(\mathcal{T}_H). \tag{3.9}$$

Since the solution may be singular at the conner points, we use the Scott–Zhang interpolation in Ω_1 instead of the Lagrange one. Let $\Pi_h : H^1(\Omega_1) \mapsto V_h$ be the Scott–Zhang interpolation (see [38,36]) so defined that the following estimates hold.

$$\begin{aligned} &|v - \Pi_h v|_{i,\mathcal{T}_h^\Gamma} \lesssim h^{2-i} |v|_{2,\mathcal{T}_h^\Gamma}, \quad 0 \leq i \leq 2, \ \forall v \in H^2(\mathcal{T}_h^\Gamma), \\ &|v - \Pi_h v|_{i,\widetilde{\mathcal{T}}_h} \lesssim h^{1+s-i} |v|_{1+s,\widetilde{\mathcal{T}}_h}, \ i = 0, 1, 0 \leq s \leq 1, \forall v \in H^{1+s}(\widetilde{\mathcal{T}}_h). \end{aligned} \tag{3.10}$$

Define the new operator $I_{h,H}$ via

$$(I_{h,H} v)|_{\Omega_1} = \Pi_h(v|_{\Omega_1}), \quad (I_{h,H} v)|_{\Omega_2} = I_H(v|_{\Omega_2}). \tag{3.11}$$

Based on the Céa Lemma 3.2 and the above approximation properties, we have the following theorem which gives the error estimate in the energy norm.

Theorem 3.1. *Let u and $u_{h,H}$ be the solutions of (2.1) and (2.9) respectively. Assume that $\forall K \in \mathcal{T}_H \cup \mathcal{T}_h^\Gamma$, $u \in H^2(K)$, and $\forall K \in \widetilde{\mathcal{T}}_h$, $u \in H^{1+s}(K)$ with some constant $0 < s \leq 1$. Then there exists a constant $\gamma_0 > 0$ independent of H, h such that when $\gamma \geq \gamma_0$, it holds that*

$$\left|\!\left|\!\left| u - u_{h,H} \right|\!\right|\!\right| \lesssim H|u|_{2,\mathcal{T}_H} + h|u|_{2,\mathcal{T}_h^\Gamma} + h^s |u|_{1+s,\widetilde{\mathcal{T}}_h}. \tag{3.12}$$

Proof. We first estimate $\left|\!\left|\!\left| u - I_{h,H} u \right|\!\right|\!\right|$. It is obvious that

$$\begin{aligned} \left|\!\left|\!\left| u - I_{h,H} u \right|\!\right|\!\right|^2 &= \left\| A^{1/2} \nabla (u - I_{h,H} u) \right\|^2_{0,\Omega_1 \cup \Omega_2} + \frac{\gamma}{H + h} \left\| [u - I_{h,H} u] \right\|^2_{0,\Gamma} \\ &\quad + \frac{H + h}{\gamma} \left\| \{ A \nabla (u - I_{h,H} u) \cdot \mathbf{n} \}_w \right\|^2_{0,\Gamma} \\ &:= \mathrm{E1} + \mathrm{E2} + \mathrm{E3}. \end{aligned}$$

From (3.9) and (3.10), we have

$$\begin{aligned} \mathrm{E1} &= \left\| A^{1/2} \nabla (u - I_H u) \right\|^2_{0,\Omega_2} + \sum_{K \in \mathcal{T}_h^\Gamma} \left\| A^{1/2} \nabla (u - \Pi_h u) \right\|^2_{0,K} \\ &\quad + \sum_{K \in \widetilde{\mathcal{T}}_h} \left\| A^{1/2} \nabla (u - \Pi_h u) \right\|^2_{0,K} \\ &\lesssim H^2 |u|^2_{2,\mathcal{T}_H} + h^2 |u|^2_{2,\mathcal{T}_h^\Gamma} + h^{2s} |u|^2_{1+s,\widetilde{\mathcal{T}}_h}. \end{aligned}$$

Further, by use of the trace inequality (3.1), we obtain

$$\begin{aligned}
\mathrm{E2} &\le 2\sum_{e\in\Gamma_h}\frac{\gamma}{H+h}\|u-\Pi_h u\|_{0,e}^2+2\sum_{E\in\Gamma_H}\frac{\gamma}{H+h}\|u-I_H u\|_{0,E}^2\\
&\lesssim \sum_{K\in\mathcal{T}_h^\Gamma} h^{-1}\big(h^{-1}\|u-\Pi_h u\|_{0,K}^2+h\|\nabla(u-\Pi_h u)\|_{0,K}^2\big)\\
&\quad+\sum_{K\in\mathcal{T}_H} H^{-1}\big(H^{-1}\|u-I_H u\|_{0,K}^2+H\|\nabla(u-I_H u)\|_{0,K}^2\big)\\
&\lesssim h^2|u|_{2,\mathcal{T}_h^\Gamma}^2+H^2|u|_{2,\mathcal{T}_H}^2.
\end{aligned}$$

Similarly, we have

$$\begin{aligned}
\mathrm{E3} &\le 2\sum_{e\in\Gamma_h}\frac{H+h}{\gamma}w_1\left\|A^{1/2}\nabla(u-\Pi_h u)\right\|_{0,e}^2\\
&\quad+2\sum_{E\in\Gamma_H}\frac{H+h}{\gamma}w_2\left\|A^{1/2}\nabla(u-I_H u)\right\|_{0,E}^2\\
&\lesssim \sum_{K\in\mathcal{T}_h^\Gamma} h\big(h^{-1}\|\nabla(u-\Pi_h u)\|_{0,K}^2+h\left\|\nabla^2(u-\Pi_h u)\right\|_{0,K}^2\big)\\
&\quad+\sum_{K\in\mathcal{T}_H} H\big(H^{-1}\|\nabla(u-I_H u)\|_{0,K}^2+H\left\|\nabla^2(u-I_H u)\right\|_{0,K}^2\big)\\
&\lesssim h^2|u|_{2,\mathcal{T}_h^\Gamma}^2+H^2|u|_{2,\mathcal{T}_H}^2.
\end{aligned}$$

Combining the estimates of E1, E2 and E3 together, we obtain

$$\left|\!\left|\!\left|u-I_{h,H}u\right|\!\right|\!\right|\lesssim H|u|_{2,\mathcal{T}_H}+h|u|_{2,\mathcal{T}_h^\Gamma}+h^s|u|_{1+s,\widetilde{\mathcal{T}}_h}.$$

Finally, by Lemma 3.2, we complete the proof of the theorem. □

4. Numerical tests

In this section, we first provide some numerical results to verify the convergence rate of the combined FEM established in Section 3. And then, we apply the combined FEM to the model problem in two kinds of domain such as the domain with the oscillating boundary on one side and the domain with the oscillating boundary on all sides to show the efficiency of the proposed method (see Figs. 3 and 5 for illustrations of such domains). For simplicity, in our numerical tests we only consider the following Poisson equation:

$$\begin{aligned}
-\Delta u &= f \quad \text{in } \Omega,\\
u &= g \quad \text{on } \partial\Omega.
\end{aligned}\tag{4.1}$$

For the combined FEM, the triangulation may be done by the same way as that of [30]. We recall the procedure as follows (see Fig. 2 for an illustration):

- First, we triangulate the domain Ω with a coarse mesh whose mesh size H is much bigger than the extent of the boundary oscillation.
- Secondly, we choose the union of coarse-grid elements adjacent to the boundary $\partial\Omega$ as Ω_1 and denote $\Omega\setminus\overline{\Omega_1}$ by Ω_2. For example, in our tests, we choose several layers of coarse-grid elements to form the domain Ω_1. It has been shown that the appropriate number of layers is determined by the decay of the H^2-norm of the exact solution away from the boundary (see [9]).
- Finally, in Ω_2, we use the linear FE basis on coarse-grid elements. While, in Ω_1 we use the linear FE basis on a fine mesh. In our tests, we use the size of the fine mesh $h=2^{-9}$ or $h=2^{-10}$ which is small enough to resolve the smallest scale of oscillations.

Remark 1. Let ε be the size of small structures of the rough boundary. According to the characterizations of the solution near the rough boundary, the width δ of the band of fine meshes can be chosen such that $\delta\gtrsim\varepsilon^\sigma$ for some constant $\sigma\in(0,1)$ (cf. [39,7]). In our numerical tests, we simply choose $\delta=H$, which is easy to be implemented.

In all of these computations, we denote the exact solution by u_e if there have. Otherwise, we use finely resolved numerical solutions obtained via the traditional linear finite element method with mesh size $h_f=2^{-10}$ as the "exact" solutions which

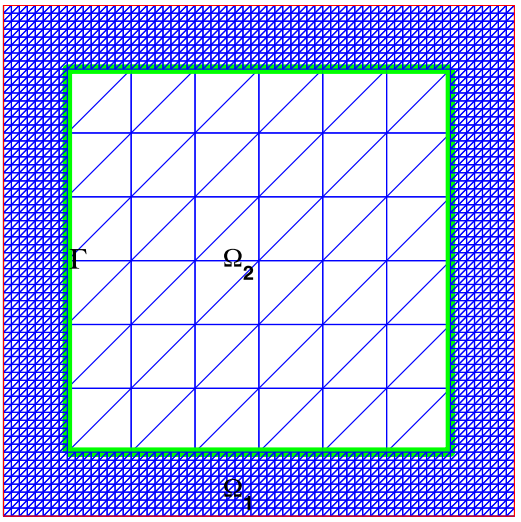

Fig. 2. A sample mesh.

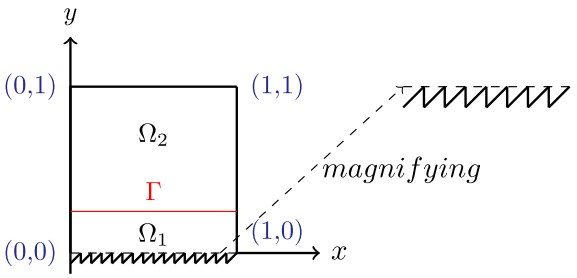

Fig. 3. The domain with rough bottom.

Table 1
Relative errors of the combined FEM for $H/h = 2^3$, $\beta = 1$, $\gamma = 200$.

H	h	L^2	Rate	L^∞	Rate	Energy error	Rate
2^{-3}	2^{-6}	2.97e−02	\	2.88e−02	\	4.73e−02	\
2^{-4}	2^{-7}	7.40e−03	2.00	7.78e−03	1.89	2.34e−02	1.02
2^{-5}	2^{-8}	1.84e−03	2.01	2.10e−03	1.89	1.17e−02	1.00
2^{-6}	2^{-9}	4.60e−04	2.00	5.70e−04	1.88	5.80e−03	1.01
2^{-7}	2^{-10}	1.15e−04	2.00	1.53e−04	1.90	2.90e−03	1.00

are still denoted as u_e. Denoting u_h as the numerical solutions computed by the methods considered in this section, we measure the relative error in L^2, L^∞ and energy norms as follows:

$$\frac{\|u_h - u_e\|_{L^2}}{\|u_e\|_{L^2}}, \quad \frac{\|u_h - u_e\|_{L^\infty}}{\|u_e\|_{L^\infty}}, \quad \frac{|||u_h - u_e|||}{|||u_e|||}.$$

4.1. Accuracy of the combined FEM

The purpose of this subsection is to verify the convergence rate of the combined FEM. To do this, we consider the model problem (4.1) in the squared domain $\Omega = [0, 1]\times[0, 1]$, the subdomains of which are $\Omega_2 := [\frac{1}{8}, \frac{7}{8}]\times[\frac{1}{8}, \frac{7}{8}]$ and $\Omega_1 := \Omega\backslash\Omega_2$ (see Fig. 2). We assume that $f = -1, g = (x^2+y^2)/4$. It is easy to check the exact solution of problem (4.1) is $u_e = (x^2+y^2)/4$, and $u_e \in H^2(\Omega)$. Recall that in Section 3, we have asserted that the energy error is bounded by $C_1H + C_2h + C_3h^s$, where s depends on the regularity of the solution. Noting here for this example, we have $s = 1$.

In our first test, we fix H/h and compute the model problem with a series of H (corresponding h). The results are listed in Table 1. We observe that the convergence rate of energy error is about 1 which is coincided with our theoretical result.

Table 2
Relative errors of the combined FEM for $h = 2^{-10}$, $\beta = 1$, $\gamma = 200$.

H	h	L^2	Rate	L^∞	Rate	Energy error	Rate
2^{-4}	2^{-10}	7.45e−03	\	7.86e−03	\	2.36e−02	\
2^{-5}	2^{-10}	1.86e−03	2.00	2.14e−03	1.88	1.17e−02	1.01
2^{-6}	2^{-10}	4.63e−04	2.01	5.76e−04	1.89	5.83e−03	1.00
2^{-7}	2^{-10}	1.15e−04	2.01	1.53e−04	1.91	2.90e−03	1.01
2^{-8}	2^{-10}	2.77e−05	2.05	4.08e−05	1.91	1.41e−03	1.04

Table 3
Relative errors of the combined FEM for $H/h = 2^3$, $\beta = 1$, $\gamma = 200$.

H	h	L^2	Rate	L^∞	Rate	Energy error	Rate
2^{-3}	2^{-6}	4.09e−02	\	8.44e−02	\	2.16e−01	\
2^{-4}	2^{-7}	1.12e−02	1.87	2.69e−02	1.65	1.13e−01	0.93
2^{-5}	2^{-8}	3.12e−03	1.84	1.02e−02	1.40	5.97e−02	0.92
2^{-6}	2^{-9}	8.39e−04	1.89	4.10e−03	1.32	3.04e−02	0.97
2^{-7}	2^{-10}	1.50e−04	2.48	6.90e−04	2.57	1.24e−02	1.29

The second test is to further verify the convergence rate with respect to H. To do this, we fix $h = 2^{-10}$ and carry on the numerical test with different H. The results are shown in Table 2. It is easy to see the convergence rate is about 1 which is also confirming our theoretical result.

4.2. Application to Poisson equation in domain with oscillating boundaries

In this subsection, we apply the combined FEM to Poisson equation on domain with oscillating boundaries. It has been shown that if the domain Ω is an arbitrary polygonal and $f \in L^p(\Omega)$, the solution u of (4.1) is always in a fractional order Sobolev space H^{1+s} for some $s \in (0, 1]$, which depends on the maximal interior angle w of Ω and p (cf. [40]). A crucial role in determining the regularity of the solution of (4.1) is played by the constant $p_w = \frac{2}{2-\frac{\pi}{w}}$. According to [40, p. 233], if $f \in L^p,\ p > 1$, then $u \in W^{2,\bar{p}}$, where

$$\bar{p} = \begin{cases} p, & \text{if} \quad p < p_w, \\ \gamma, \quad \text{any } \gamma < p_w, & \text{if} \quad p \geq p_w, \end{cases} \qquad p_w = \frac{2}{2 - \frac{\pi}{w}}.$$

By the imbedding theorem, $W^{2,\bar{p}} \subset H^{1+s}$, for $s = 2 - \frac{2}{\bar{p}}$, we obtain the following result:

$$\text{If } f \in L^p,\ p > 1,\ \text{then } u \in H^{1+s},\ s = 2 - \frac{2}{\bar{p}}. \tag{4.2}$$

We will implement three examples with different oscillating boundaries in this subsection. In the first example, we assume that the domain Ω is a rectangle with a rough bottom, as depicted in Fig. 3. The rough domain is given by

$$\Omega := \{x \in \mathbb{R}^2 \mid 0 < x_1 < 1,\ \gamma_1(x) < x_2 < 1\},$$

where $\gamma_1(x)$ is a periodic function with period equal to $1/16$. In one period, fox example, when $x_1 \in (0,\ 1/16)$, $\gamma_1(x)$ is a line segment from $(0,\ -1/16)$ to $(1/16,\ 0)$. We choose $f = 1$ in (4.1), and set homogeneous Dirichlet boundary condition on $\partial\Omega$. It is easy to see that the maximal interior angle w of this example is $\frac{7}{4}\pi$. Therefore, according to (4.2), the solution u belongs to $H^{11/7-\delta}(\Omega)$ for some arbitrary small positive constant δ. In this example, we set

$$\Omega_1 := \{x \in \mathbb{R}^2 \mid 0 < x_1 < 1,\ \gamma(x) < x_2 < 0.125\},$$

and

$$\Omega_2 := \{x \in \mathbb{R}^2 \mid 0 < x_1 < 1,\ 0.125 < x_2 < 1\}.$$

The coarse-fine mesh interface Γ is defined by

$$\Gamma = \{x \in \mathbb{R}^2 \mid 0 < x_1 < 1,\ x_2 = 0.125\}.$$

We use mesh sizes h and H in the subdomain Ω_1 and Ω_2 respectively.

For the first example, we design three series of tests. Firstly, we fix H/h and compute the problem with a series of H (corresponding h). The results are listed in Table 3. We observe that the convergence rate of energy error is less than 1. The optimal convergence rate cannot be obtained due to the low regularity of the solution. This observation accords with our theoretical result.

Secondly, in order to make the convergence rate dependency relationship with respect to the regularity of the solution more clear, we fix $h = 2^{-10}$, and carry on the numerical test with different H. The results are shown in Table 4. It is easy to see the convergence rate of energy error is about 1 which is coincided with our theoretical result.

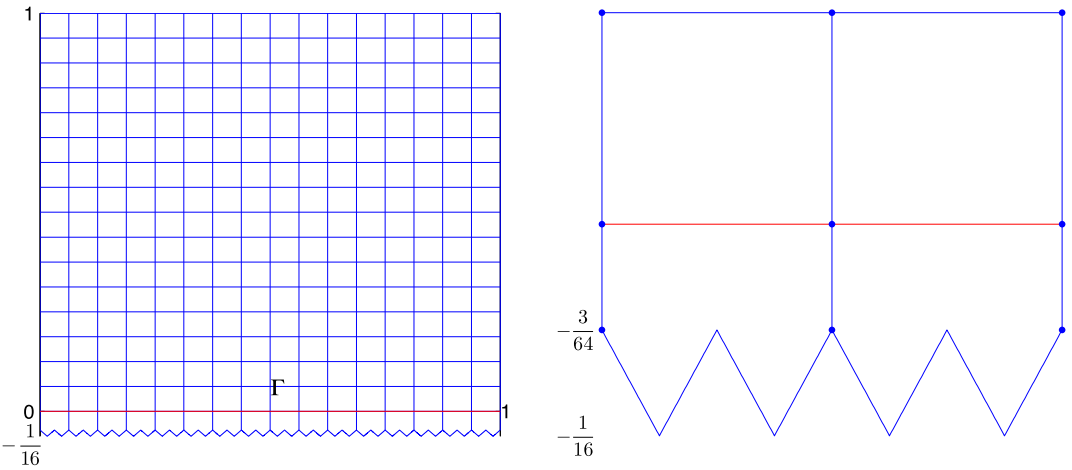

Fig. 4. Left: a mesh for Ω. Right: a patch of elements intercepting Γ.

Table 4
Relative errors of the combined FEM for $h = 2^{-10}$, $\beta = 1$, $\gamma = 200$.

H	h	L^2	Rate	L^∞	Rate	Energy error	Rate
2^{-4}	2^{-10}	9.66e−03	\	2.69e−02	\	9.98e−02	\
2^{-5}	2^{-10}	2.43e−03	1.99	8.17e−03	1.72	5.00e−02	1.00
2^{-6}	2^{-10}	6.06e−04	2.00	2.40e−03	1.77	2.49e−02	1.01
2^{-7}	2^{-10}	1.50e−04	2.01	6.90e−04	1.80	1.24e−02	1.01
2^{-8}	2^{-10}	3.60e−05	2.06	1.94e−04	1.83	6.02e−03	1.04

Table 5
Relative errors of the combined FEM for $H = 2^{-10}$, $\beta = 1$, $\gamma = 200$.

H	h	L^2	Rate	L^∞	Rate	Energy error	Rate
2^{-10}	2^{-4}	2.95e−02	\	6.34e−02	\	1.86e−01	\
2^{-10}	2^{-5}	1.48e−02	1.00	3.87e−02	0.71	1.24e−01	0.58
2^{-10}	2^{-6}	6.99e−03	1.08	2.63e−02	0.56	8.08e−02	0.62
2^{-10}	2^{-7}	3.09e−03	1.18	1.72e−02	0.61	5.25e−02	0.62
2^{-10}	2^{-8}	1.24e−03	1.32	1.02e−02	0.75	3.26e−02	0.69

Finally, we fix $H = 2^{-10}$, and simulate the problem with different h. The results are listed in Table 5. We find that the convergence rate in energy error with respect to h is almost 0.6, which is close to 4/7, and then also accords with our theoretical result.

The second example is designed to show the proposed method is competitive. As the first example, we assume that the domain Ω is a rectangle with a rough bottom, as depicted in Fig. 4. The rough domain is given by

$$\Omega := \{x \in \mathbb{R}^2 | 0 < x_1 < 1, \gamma_2(x) < x_2 < 1\},$$

where $\gamma_2(x)$ is a periodic function with period equal to 1/32.

In one period, e.g., when $x_1 \in (0, 1/32)$, $\gamma_2(x)$ is a broken line from $(0, -3/64)$ to $(1/64, -1/16)$, and from $(1/64, -1/16)$ to $(1/32, -3/64)$. We choose $f = 1$ in (4.1), and set homogeneous Dirichlet boundary condition on $\partial\Omega$. In order to illustrate the performance of our method, we implement the MsFEM introduced in [7]. Note for the first example, the MsFEM introduced in [7] is inapplicable since the cell problem is not well-defined. The relative errors about L^2, L^∞, and energy norm of which are listed in Table 6. We observe that the combined FEM gives much better approximation than the MsFEM in [7]. We also compare the CPU times T_1 and T_2 spent by the methods considered here, where T_1 is the CPU time of computing the multiscale basis functions, and T_2 is the CPU time of assembling the stiffness matrix and solving the discretized system of algebraic equations. For the combined method, there is no need to compute the basis functions. However, the CPU time T_2 is a little longer than that of the MsFEM. We remark that the CPU time T_2 can be shortened further by applying more efficient FEM in the problematic region.

In the last example, we consider a more general domain with arbitrary oscillating boundaries on all sides (see Fig. 5). The extent of the boundary oscillation is $\frac{1}{64}$. In the simulation, we fix the fine mesh size $h = 2^{-9}$, and employ the combined FEM to test the convergence rate with respect to H. The results illustrated in Table 7 show the efficiency of the proposed method. It also turns out that the convergence rate of the energy error with respect to H is about 1 which agree with the theoretical result.

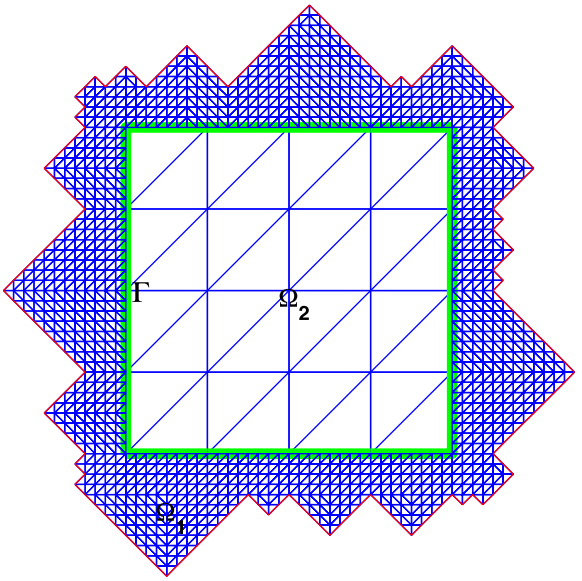

Fig. 5. Domain with oscillating boundaries on all sides.

Table 6
Relative errors of the combined FEM with $\beta = 1$, $\gamma = 200$, $H = 2^{-4}$, $h = 2^{-10}$ versus relative errors of MsFEM in [7] with $H = 2^{-4}$.

Relative error	L^2	L^∞	Energy	CPU time (s)	
				T_1	T_2
MsFEM	7.514e−01	7.506e−01	7.519e−01	1.61e−00	2.62e−02
combined FEM	1.032e−02	2.605e−02	8.034e−02	0	4.12e−01

Table 7
Relative errors of the combined FEM for $\beta = 1$, $\gamma = 200$.

H	h	L^2	Rate	L^∞	Rate	Energy error	Rate
2^{-4}	2^{-9}	1.07e−02	\	2.02e−02	\	2.42e−02	\
2^{-5}	2^{-9}	2.68e−03	2.00	5.44e−03	1.89	1.20e−02	1.01
2^{-6}	2^{-9}	6.65e−04	2.01	1.46e−03	1.90	5.95e−03	1.01
2^{-7}	2^{-9}	1.60e−04	2.06	3.93e−04	1.89	2.90e−03	1.04
2^{-8}	2^{-9}	3.44e−05	2.22	1.05e−04	1.90	1.30e−03	1.16

5. Conclusion

In this paper, we have developed a combined FEM for the elliptic problems posted in domains with oscillating boundaries. The main purpose of this paper is to better approximate the singular features that occur in the vicinity of oscillating boundaries. To aim this goal, we first separate the research domain into two parts Ω_1 and $\Omega_2 = \Omega \setminus \overline{\Omega_1}$ that Ω_1 contains the regions where we need a very fine mesh to resolve it. Then we use the linear FEM on a fine mesh of Ω_1 while use the linear FEM on a coarse mesh of Ω_2 to reduce unnecessary computational effort. In addition, we deal with the transmission condition on the interface $\Gamma = \partial\Omega_1 \cap \partial\Omega_2$ by penalizing the jumps from the linear function values of the discrete solution. The interesting part of the proposed method lies in the new scheme employing a weighted average in the definition of the bilinear form, which avoiding the affection of the ratio of the sizes of the coarse and fine meshes.

A rigorous and careful analysis has been given for elliptic equations with general coefficients and oscillating boundaries to show the consistence, stability, and convergence of the numerical scheme. Since in different place the solution of the equation may have different regularity, the error estimate is expanded in terms of elements, from which actually we get the quasi-optimal convergence.

Numerical experiments are carried out for Poisson equation with regular boundary, oscillating boundary on one side or all sides to verify the theoretical findings. The numerical results demonstrate the accuracy and efficiency of the proposed method. We also compute the convergence rate in energy error with respect to H and h respectively. All of the numerical results are coincided with the theoretical results.

We remark that the condition number of the combined FEM depends on H, h, d, and the thickness of the fine-mesh region Ω_1 (denoted by δ). For example, in two dimensional case, the condition number is $O\big(H^{-2} + (h/\delta)^{-2}\big)$. Clearly, if $\delta \lesssim h/H$,

the condition number is $O(H^{-2})$. Since the thickness of the fine-mesh domain is usually small, the very fine mesh near the boundary does not cause problem in the computations. In our tests, the condition number is about $10^5 \sim 10^6$. More details about the estimate of the condition number are arranged in the Appendix.

The combined FEM may be applied into many other singular problems, e.g., the porous media with channelized structure, or in near-well region. It is also possible to combine the oversampling MsFEM with the linear FEM on a very fine mesh of the problematic portion to deal with the problems with both oscillating coefficients and oscillating boundaries.

Compared with the standard FEM on adaptively refined mesh, our combined FEM does not require the buffer zone with gradually changing mesh size to connect the very fine mesh zone and the very coarse mesh zone, and therefore, needs smaller number of DOFs to achieve the same accuracy. When the regularity estimates of the solution near the rough boundary are known priorly, the interface Γ and the meshes sizes can also be determined priorly, and there is no need to compute the posteriori error estimators as the adaptive FEM, which also saves some CPU time. But when the singularities of the solution are unknown, we have to develop adaptive algorithm for the combined FEM to achieve the quasi-optimal computational complexity. This will be done in a future work.

Acknowledgments

The authors would like to thank the referees for their careful reading and constructive comments that improved the paper.

The work of first and second authors was partially supported by the NSF of China grant 10971096, and by the Project Funded by the Priority Academic Program Development of Jiangsu Higher Education Institutions. The work of third author was partially supported by the NSF of China grants 11525103, 91130004.

Appendix. Estimate of the condition number

In this appendix, we estimate the condition number of the stiffness matrix of the combined FEM. Recall that $\Omega_2 \subset\subset \Omega$ and $\Omega = \Omega_1 \cup \Omega_2 \cup \Gamma$, where $\Gamma = \partial\Omega_1 \cap \partial\Omega_2$ is the interface of Ω_1 and Ω_2.

Lemma A.1. *Suppose that* $\mathrm{dist}(x, \Gamma) \le \delta$ *for any* $x \in \partial\Omega$ *and some constant* $\delta > 0$. *Then for all* $w \in \{w : w_i = w|_{\Omega_i} \in H^1(\Omega_i), i = 1, 2, w|_{\partial\Omega} = 0\}$, *it holds:*

$$\delta^{-1}\|w\|_{0,\Omega_1} + \|w\|_{0,\Omega_2} \lesssim \|\nabla w\|_{0,\Omega_1\cup\Omega_2} + \|[w]\|_{0,\Gamma}.$$

Proof. Since $w_1|_{\partial\Omega} = 0$, from the Friedrichs' inequality, we have

$$\|w_1\|_{0,\Omega_1} \lesssim \delta\|\nabla w_1\|_{0,\Omega_1}. \tag{A.1}$$

On the other hand, the norm-equivalent-theorem implies that

$$\|w_2\|_{0,\Omega_2} \lesssim \|\nabla w_2\|_{0,\Omega_2} + \|w_2\|_{0,\Gamma}. \tag{A.2}$$

From the trace inequality, it follows that

$$\begin{aligned}\|w_2\|_{0,\Gamma} &\le \|[w]\|_{0,\Gamma} + \|w_1\|_{0,\Gamma}\\ &\lesssim \|[w]\|_{0,\Gamma} + \delta^{-1/2}\|w_1\|_{0,\Omega_1} + \delta^{1/2}\|\nabla w_1\|_{0,\Omega_1},\end{aligned}$$

which combining (A.1) and (A.2), yields the result. □

Theorem A.1. *Let A be the stiffness matrix of the combined FEM (2.9). Then*

$$\mathrm{cond}(A) \lesssim (H/h)^{d-2}(H^{-2} + (h/\delta)^{-2}). \tag{A.3}$$

Proof. Let $\{\phi_1, \phi_2, \ldots, \phi_m\}$ and $\{\phi_{m+1}, \phi_{m+2}, \ldots, \phi_n\}$ be the bases of V_H and V_h respectively. For any $v_{h,H} \in V_{h,H}$, we have $v_{h,H} = v_1\phi_1 + \cdots + v_n\phi_n$. Denote $v = (v_1, \ldots, v_n)^T$. Hence $a(v_{h,H}, v_{h,H}) = v^T A v$, where $A = (a(\phi_j, \phi_i))_{n\times n}$.

Denote by $\|v_{h,H}\|_{0*}^2 = (H/h)^2\|v_h\|_{0,\Omega_1}^2 + \|v_H\|_{0,\Omega_2}^2$. It is obvious that

$$\frac{v^T A v}{v^T v} = \frac{a(v_{h,H}, v_{h,H})}{\|v_{h,H}\|_{0*}^2}\frac{\|v_{h,H}\|_{0*}^2}{v^T v}. \tag{A.4}$$

Thus, it suffices to estimate $\frac{a(v_{h,H}, v_{h,H})}{\|v_{h,H}\|_{0*}^2}$ and $\frac{\|v_{h,H}\|_{0*}^2}{v^T v}$. From the definition of energy norm $|||\cdot|||$, it follows that

$$\begin{aligned}\left|\left|\left|v_{h,H}\right|\right|\right| &\lesssim (1+\gamma^{-1})\|\nabla v_{h,H}\|_{0,\Omega_1\cup\Omega_2}^2 + \gamma(H+h)^{-1}\|[v_{h,H}]\|_{0,\Gamma}^2\\ &\lesssim h^{-2}\|v_h\|_{0,\Omega_1}^2 + H^{-2}\|v_H\|_{0,\Omega_2}^2\\ &\quad + (H+h)^{-1}h^{-1}\|v_h\|_{0,\Omega_1}^2 + (H+h)^{-1}H^{-1}\|v_H\|_{0,\Omega_2}^2\\ &\lesssim H^{-2}\left((H/h)^2\|v_h\|_{0,\Omega_1}^2 + \|v_H\|_{0,\Omega_2}^2\right).\end{aligned} \tag{A.5}$$

Further, from Lemma A.1, we have

$$\begin{aligned}(H/h)^2\|v_h\|_{0,\Omega_1}^2+\|v_H\|_{0,\Omega_2}^2 &\lesssim \left((H\delta/h)^2+1\right)\left(\|\nabla v_{h,H}\|_{0,\Omega_1\cup\Omega_2}+\|[v_{h,H}]\|_{0,\Gamma}\right)\\ &\lesssim \left(1+\gamma(H+h)^{-1}\right)\left((H\delta/h)^2+1\right)\left|\!\left|\!\left|v_{h,H}\right|\!\right|\!\right|^2 \\ &\lesssim \left((H\delta/h)^2+1\right)a(v_{h,H},v_{h,H}).\end{aligned} \tag{A.6}$$

From (A.5) and (A.6), we conclude that

$$\left(1+(H\delta/h)^2\right)^{-1}\lesssim \frac{a(v_{h,H},v_{h,H})}{\|v_{h,H}\|_{0*}^2}\lesssim H^{-2}. \tag{A.7}$$

Next, we estimate $\frac{\|v_{h,H}\|_{0*}^2}{v^Tv}$. It is easy to see that

$$\begin{aligned}\|v_{h,H}\|_{0*}^2 &= \|v_H\|_{0,\Omega_2}^2+(H/h)^2\|v_h\|_{0,\Omega_1}^2\\ &\eqsim H^d\sum_{i=1}^{m}|v_i|^2+(H/h)^2h^d\sum_{i=m+1}^{n}|v_i|^2,\end{aligned}$$

which implies that

$$H^2h^{d-2}\lesssim \frac{\|v_{h,H}\|_{0*}^2}{v^Tv}\lesssim H^d. \tag{A.8}$$

From (A.4), (A.7) and (A.8), it follows that

$$\frac{H^2h^{d-2}}{1+(H\delta/h)^2}\lesssim \frac{v^TAv}{v^Tv}\lesssim H^{d-2}.$$

Finally, we conclude that

$$\begin{aligned}\mathrm{cond}(A) &\lesssim (1+(H\delta/h)^2)(H/h)^{d-2}H^{-2}\\ &\lesssim (H/h)^{d-2}(H^{-2}+(h/\delta)^{-2}).\end{aligned}$$

This completes the proof of the theorem. □

References

[1] Y. Amirat, O. Bodart, G.A. Chechkin, A.L. Piatnitski, Boundary homogenization in domains with randomly oscillating boundary, Stochastic Process. Appl. 121 (1) (2011) 1–23.
[2] A. Voronovich, Wave Scattering From Rough surfaces, second ed., Springer-Verlag, Berlin Heidelberg, 1999.
[3] W. Jäger, A. Mikelić, On the roughness-induced effective boundary conditions for an incompressible viscous flow, J. Differential Equations 170 (1) (2001) 96–122.
[4] D. Blanchard, L. Carbone, A. Gaudiello, Homogenization of a monotone problem in a domain with oscillating boundary, M2AN Math. Model. Numer. Anal. 33 (5) (1999) 1057–1070.
[5] I.S. Malakhova, A boundary value problem for an elliptic equation with rapidly oscillating coefficients in a rectangle, Zh. Vychisl. Mat. Mat. Fiz. 51 (8) (2011) 1457–1466.
[6] D. Borisov, G. Cardone, L. Faella, C. Perugia, Uniform resolvent convergence for strip with fast oscillating boundary, J. Differential Equations 255 (12) (2013) 4378–4402.
[7] A.L. Madureira, A multiscale finite element method for partial differential equations posed in domains with rough boundaries, Math. Comp. 78 (265) (2009) 25–34.
[8] P. Ming, X. Xu, A multiscale finite element method for oscillating Neumann problem on rough domain, Multiscale Model. Simul. 14 (4) (2016) 1276–1300.
[9] D. Elfverson, M.G. Larson, A. Målqvist, Multiscale methods for problems with complex geometry, Comput. Methods Appl. Mech. Engrg. 321 (2017) 103–123.
[10] T.Y. Hou, X.H. Wu, A multiscale finite element method for elliptic problems in composite materials and porous media, J. Comput. Phys. 134 (1) (1997) 169–189.
[11] J.F. Bonder, R. Orive, J.D. Rossi, The best Sobolev trace constant in a domain with oscillating boundary, Nonlinear Anal. 67 (4) (2007) 1173–1180.
[12] I. Babuška, M. Zlámal, Nonconforming elements in the finite element method with penalty, SIAM J. Numer. Anal. 10 (5) (1973) 863–875.
[13] G. Baker, Finite element methods for elliptic equations using nonconforming elements, Math. Comp. 31 (1977) 44–59.
[14] J. Douglas Jr., T. Dupont, Interior Penalty Procedures for Elliptic and Parabolic Galerkin methods, in: Lecture Notes in Phys., vol. 58, Springer-Verlag, Berlin, 1976.
[15] M.F. Wheeler, An elliptic collocation-finite element method with interior penalties, SIAM J. Numer. Anal. 15 (1978) 152–161.
[16] D. Arnold, An interior penalty finite element method with discontinuous elements, SIAM J. Numer. Anal. 19 (1982) 742–760.
[17] D. Arnold, F. Brezzi, B. Cockburn, D. Marini, Unified analysis of discontinuous Galerkin methods for elliptic problems., SIAM J. Numer. Anal. 39 (2001) 1749–1779.
[18] O.A. Karakashian, F. Pascal, A posteriori error estimates for a discontinuous Galerkin approximation of second-order elliptic problems, SIAM J. Numer. Anal. 41 (6) (2003) 2374–2399 (electronic).
[19] E. Burman, S. Claus, P. Hansbo, M.G. Larson, A. Massing, CutFEM: discretizing geometry and partial differential equations, Internat. J. Numer. Methods Engrg. 104 (7) (2015) 472–501.

[20] T.P. Fries, T. Belytschko, The extended/generalized finite element method: an overview of the method and its applications, Internat. J. Numer. Methods Engrg. 84 (3) (2010) 253–304.
[21] W. Hackbusch, S.A. Sauter, Composite finite elements for the approximation of PDEs on domains with complicated micro-structures, Numer. Math. 75 (4) (1997) 447–472.
[22] M. Rech, S. Sauter, A. Smolianski, Two-scale composite finite element method for Dirichlet problems on complicated domains, Numer. Math. 102 (4) (2006) 681–708.
[23] D. Peterseim, S.A. Sauter, The composite mini element-coarse mesh computation of Stokes flows on complicated domains, SIAM J. Numer. Anal. 46 (6) (2008) 3181–3206.
[24] D. Peterseim, S.A. Sauter, Finite element methods for the Stokes problem on complicated domains, Comput. Methods Appl. Mech. Engrg. 200 (33–36) (2011) 2611–2623.
[25] C.-C. Chu, I.G. Graham, T.-Y. Hou, A new multiscale finite element method for high-contrast elliptic interface problems, Math. Comp. 79 (272) (2010) 1915–1955.
[26] Y. Efendiev, J. Galvis, X.H. Wu, Multiscale finite element methods for high-contrast problems using local spectral basis functions, J. Comput. Phys. 230 (4) (2011) 937–955.
[27] Z. Chen, X.Y. Yue, Numerical homogenization of well singularities in the flow transport through heterogeneous porous media, Multiscale Model. Simul. 1 (2003) 260–303.
[28] P. Henning, D. Peterseim, Oversampling for the multiscale finite element method, Mutliscale Model. Simul. 11 (4) (2013) 1149–1175.
[29] E.T. Chung, Y. Efendiev, G. Li, An adaptive GMsFEM for high-contrast flow problems, J. Comput. Phys. 273 (2014) 54–73.
[30] W. Deng, H. Wu, A combined finite element and multiscale finite element method for the multiscale elliptic problems, Multiscale Model. Simul. 12 (4) (2014) 1424–1457.
[31] E. Rank, R. Krause, A multiscale finite-element method, Comput. Struct. 64 (1) (1997) 139–144.
[32] A. Målqvist, D. Peterseim, Localization of elliptic multiscale problems, Math. Comp. 83 (290) (2014) 2583–2603.
[33] D. Elfverson, E.H. Georgoulis, A. Målqvist, D. Peterseim, Convergence of a discontinuous Galerkin multiscale method, SIAM J. Numer. Anal. 51 (6) (2013) 3351–3372.
[34] D. Elfverson, V. Ginting, P. Henning, On multiscale methods in Petrov-Galerkin formulation, Numer. Math. 131 (4) (2015) 643–682.
[35] P. Henning, A. Målqvist, Localized orthogonal decomposition techniques for boundary value problems, SIAM J. Sci. Comput. 36 (4) (2014) A1609–A1634.
[36] S. Brenner, L. Scott, The Mathematical Theory of Finite Element Methods, third ed., Springer-Verlag, 2008.
[37] P.G. Ciarlet, The Finite Element Method for Elliptic Problems, in: Studies in Mathematics and its Applications, vol. 4, North-Holland Publishing Co., Amsterdam-New York-Oxford, 1978, p. xix+530.
[38] L. Scott, S. Zhang, Finite element interpolation of nonsmooth functions satisfying boundary conditions, Math. Comp. 54 (1990) 483–493.
[39] A. Madureira, F. Valentin, Asymptotics of the Poisson problem in domains with curved rough boundaries, SIAM J. Math. Anal. 38 (2007) 1450–1473.
[40] P. Grisvard, Elliptic Problems in Nonsmooth Domains, Pitman, Boston, 1985.